ACCSCIENCE PUBLISHING

Innovative Medicines & Omics

ORIGINAL RESEARCH ARTICLE

In silico comparative drug repurposing analysis of selected antifungal agents against SARS-CoV-2 main protease (Mpro, PDB ID: 6LU7): Molecular docking, ADMET profiling, and drug-likeness evaluation

Mohd Sameer*

College of Biotechnology, Sardar Vallabhbhai Patel University of Agriculture and Technology, Meerut, Uttar Pradesh, India

Abstract

SARS-CoV-2 main protease (Mpro, 3CLpro, PDB ID: 6LU7) cleaves viral polyproteins pp1a and pp1ab at 11 conserved recognition sites, releasing the non-structural proteins needed for replication–transcription complex assembly. Its catalytic HIS41-CYS145 dyad lacks a close human homolog, providing Mpro with a reasonable selectivity window as a drug target. Four approved antifungal azoles—posaconazole, itraconazole, fluconazole, and ketoconazole—were evaluated in this study as candidate non-covalent inhibitors against the 6LU7 crystal structure (2.16 Å) using AutoDock Vina v1.2.5 under rigid-receptor conditions. GC-376, a non-covalent Mpro inhibitor with published IC_{50} data, was docked under identical conditions and served as the primary scoring reference (ΔG = −6.763 kcal/mol). Nirmatrelvir was retained solely for the mechanistic context; rigid non-covalent docking cannot model its CYS145-alkylating mechanism. Posaconazole returned the strongest predicted affinity (−8.288 kcal/mol), followed by itraconazole (−8.095 kcal/mol), fluconazole (−5.068 kcal/mol), nirmatrelvir (−4.370 kcal/mol), and ketoconazole (−3.769 kcal/mol). Posaconazole occupied the HIS41-CYS145 catalytic cleft with predicted contacts at MET49 (~3.8 Å), MET165 (~4.1 Å), GLU166 (~3.3 Å), and the catalytic dyad residues HIS41 (~3.2 Å) and CYS145 (~3.5 Å). These distances were estimated from a rigid-receptor protocol and carry inherent coordinate uncertainty; they are not experimentally validated geometries. Posaconazole and itraconazole both carry multiple Lipinski violations, elevated lipophilicity (LogP > 4.5), predicted hERG II inhibition, and hepatotoxicity risk. Fluconazole showed a clean absorption, distribution, metabolism, excretion, and toxicity (ADMET) profile, with weaker predicted binding (−5.068 kcal/mol). No antiviral activity was claimed. Molecular dynamics simulation, binding free energy calculation, and *in vitro* Mpro inhibition assays are required before any biological inference can be drawn.

Keywords: SARS-CoV-2; Mpro; Molecular docking; Drug repurposing; Antifungal azoles; Absorption, distribution, metabolism, excretion, and toxicity profiling; Interaction distances

***Corresponding author:**
Mohd Sameer
(sameer7419@svpuat.edu.in)

Citation: Sameer M. *In silico* comparative drug repurposing analysis of selected antifungal agents against SARS-CoV-2 main protease (Mpro, PDB ID: 6LU7): Molecular docking, ADMET profiling, and drug-likeness evaluation. *Innov Med Omics.* 2026;3(4):026190022. doi: 10.36922/IMO026190022

Received: May 8, 2026

Revised: May 24, 2026

Accepted: June 1, 2026

Published online: June 23, 2026

Copyright: © 2026 Author(s). This is an Open-Access article distributed under the terms of the Creative Commons Attribution License, permitting distribution, and reproduction in any medium, provided the original work is properly cited.

Publisher's Note: AccScience Publishing remains neutral with regard to jurisdictional claims in published maps and institutional affiliations.

1. Introduction

SARS-CoV-2 emerged in late 2019, with no approved antiviral available.[1] Its main protease (Mpro, 3CLpro) attracted rapid attention from drug-discovery groups worldwide. The enzyme cleaves viral polyproteins pp1a and pp1ab at 11 conserved recognition sequences, releasing non-structural proteins 4–16 that assemble the replication–transcription complex.[2,3] Inhibiting the enzyme stalls viral replication at the polyprotein stage.

The Mpro protein functions as a homodimer. Each monomer presents a HIS41-CYS145 catalytic dyad at the substrate-binding cleft. This catalytic dyad resembles, but is structurally distinct from, human cysteine proteases—a divergence that supports the selectivity of Mpro-targeted therapeutics.[4] Jin *et al.*[5] deposited the first high-resolution co-crystal structure (PDB: 6LU7; 2.16 Å) within weeks of the pandemic declaration, and this structure became the standard reference for computational screening campaigns.

Nirmatrelvir (PF-07321332), the reversible covalent peptidomimetic in Paxlovid®, validated the target clinically.[6] Its approval showed that Mpro inhibition produces measurable antiviral benefit in patients. At the same time, it left open questions about non-covalent chemotypes—in particular, whether scaffolds from other therapeutic areas could be repositioned more quickly.

Drug repurposing is attractive during a pandemic because approved agents already have safety and pharmacokinetic data, thereby compressing preclinical timelines.[7] Antifungal azoles have been proposed as repurposing candidates across several viral targets; azole nitrogen atoms can engage enzyme binding pockets in ways broadly compatible with known inhibitor geometries.[8] Four azoles were deliberately selected to span the physicochemical range of the class: posaconazole and itraconazole (molecular weight [MW] > 700 g/mol, logP > 4.5), fluconazole (306 g/mol, logP 0.73), and ketoconazole, which already carries documented CYP inhibitory and hepatotoxic liabilities.[9]

Individual azoles have been reported in SARS-CoV-2 docking studies before,[10] but a side-by-side comparison of all four under one protocol—with a validated non-covalent reference and parallel absorption, distribution, metabolism, excretion, and toxicity (ADMET) profiling—has not been reported. Studies that relied on nirmatrelvir as the sole benchmark introduced a mechanistic mismatch: nirmatrelvir's potency depends on covalent CYS145 alkylation rather than non-covalent affinity. GC-376 provides a more appropriate comparator for non-covalent inhibition of Mpro.

Three methodological choices defined this study. GC-376, with published enzymatic IC_{50} data,[11] was docked under identical conditions and treated as the primary scoring reference. Nirmatrelvir was retained as a mechanistic comparator. All docking results were interpreted conservatively: ΔG values were structural hypotheses, not activity predictions, and the interpretive distance from any clinical claim is stated explicitly throughout.

A secondary pattern also informs this study's design. Larger, more lipophilic scaffolds exhibit higher docking scores in Vina's empirical scoring function, but these advantages do not necessarily reflect superior binding geometry once lipophilicity bias and molecular size effects are corrected.[12] Fluconazole illustrates the inverse problem: acceptable ADMET properties paired with affinity below the GC-376 baseline. This tension is a documented pattern in computational repurposing, and the four-compound dataset here provides a case study with explicit quantification.

The protocol is reproducible: AutoDock Vina v1.2.5, MMFF94-minimized ligands from PubChem, identical grid parameters, parallel SwissADME/pkCSM profiling, and conservative interpretation throughout.

2. Materials and methods

Figure 1 presents the complete seven-step computational workflow. Each step is described below.

2.1. Target protein retrieval and preparation

The SARS-CoV-2 Mpro crystal structure (PDB ID: 6LU7; resolution 2.16 Å) was retrieved from the Research Collaboratory for Structural Bioinformatics (RCSB) Protein Data Bank.[13,14] The co-crystallized ligand N3, all heteroatom groups, and crystallographic water molecules were removed. Polar hydrogen atoms were added, and Gasteiger–Marsili partial charges were assigned using AutoDockTools (MGLTools v1.5.7).[15] The processed receptor was exported in PDBQT format. All residues were held rigid; induced-fit effects at the S2 loop (residues 45–52) are a recognized source of uncertainty that ensemble docking methods can partially address.[4]

2.2. Ligand preparation

Three-dimensional structures of posaconazole (CID: 147696), itraconazole (CID: 55283), fluconazole (CID: 3365), ketoconazole (CID: 456201), nirmatrelvir (CID: 145996610), and GC-376 (CID: 46943432) were retrieved from PubChem as SDF files.[16] GC-376 was prepared under the same protocol as the test compounds and designated the primary non-covalent benchmark.

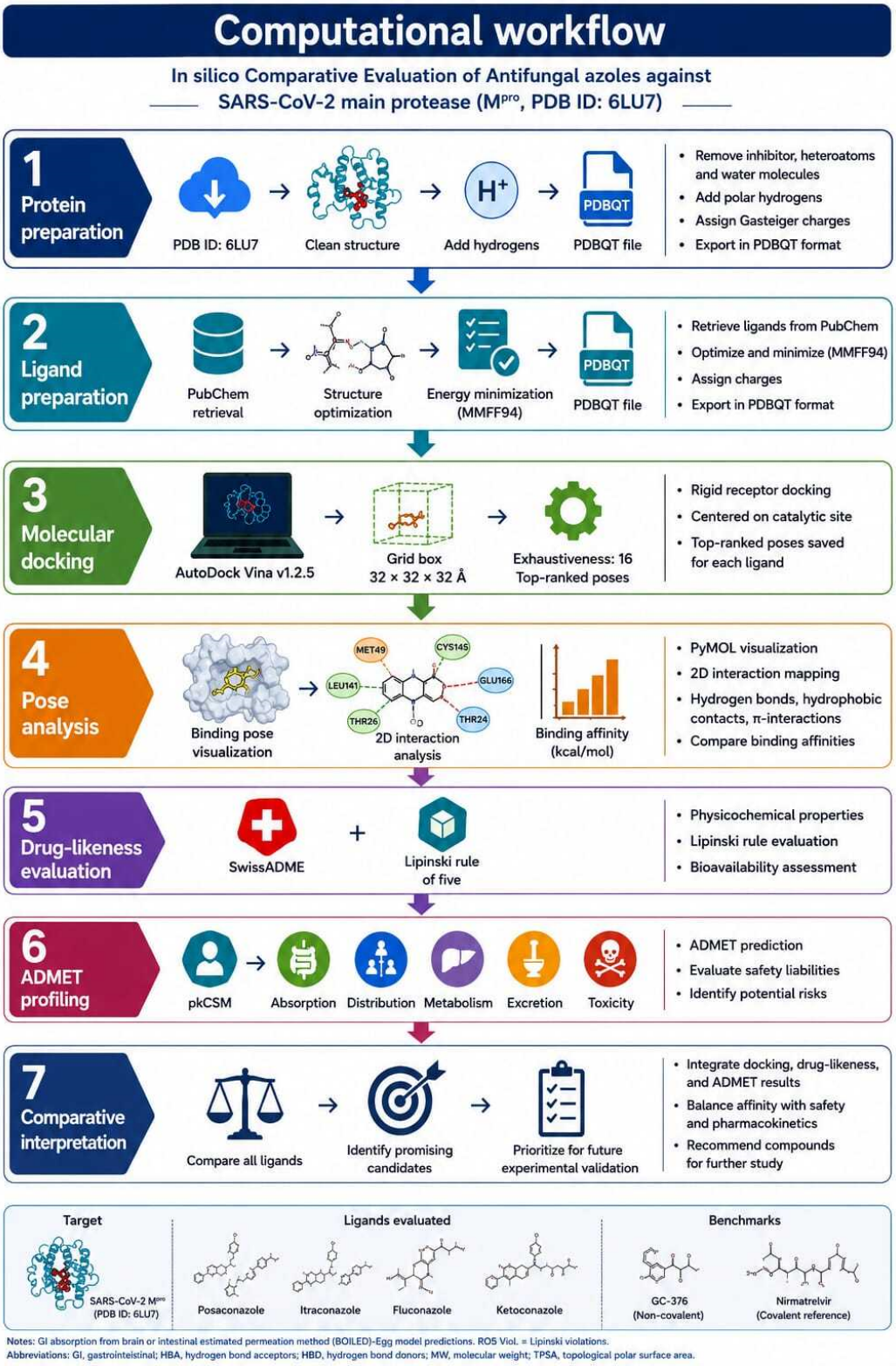


Figure 1. Computational workflow summarizing the seven sequential steps applied in this study: protein retrieval and preparation; ligand preparation; molecular docking; pose visualization and interaction analysis; drug-likeness evaluation; absorption, distribution, metabolism, excretion, and toxicity (ADMET) profiling; and comparative interpretation

Conformer generation and force-field minimization were performed using Open Babel v3.1.1[17] with the MMFF94 parameter set (convergence: 10^{-4} kcal/mol/Å). Gasteiger charges were computed in MGLTools v1.5.7 before PDBQT conversion. All six compounds were processed identically.

2.3. Molecular docking protocol

Docking was performed using AutoDock Vina v1.2.5.[18] The grid box was centered on the substrate-binding cleft at ($x = -26$, $y = 12$, $z = 58$) Å, with a cubic search volume of 32 × 32 × 32 Å encompassing the S1, S2, and S3 sub-pockets. Exhaustiveness was set to 16. The top-ranked pose per compound was retained. Vina's scoring function evaluates van der Waals, hydrogen bond, hydrophobic, and torsional terms; it does not model covalent bond formation.

2.4. Pose visualization and interaction analysis

Docked complexes were visualized in PyMOL v2.5.[19] Residues within approximately 5 Å of each top-ranked pose were identified. Interaction types were assigned based on visual inspection of the known sub-pocket architecture.[4] Estimated interaction distances were read from the PyMOL distance measurement tool on the top-ranked rigid-docked pose. These values carry inherent coordinate uncertainty and are reported as approximate estimates, not experimentally validated measurements.

2.5. Drug-likeness and absorption, distribution, metabolism, excretion, and toxicity profiling

Drug-likeness parameters were obtained from SwissADME.[20] Parameters recorded included MW, logP, hydrogen bond donors (HBD), hydrogen bond acceptors (HBA), topological polar surface area (TPSA), and Lipinski rule-of-five (RO5) compliance.[21] The brain or intestinal estimated permeation method (BOILED)-Egg model assessed predicted gastrointestinal absorption and blood–brain barrier penetration.[22] ADMET properties were predicted using pkCSM.[23] Parameters included intestinal absorption, P-glycoprotein (P-gp) substrate status, cytochrome P450 (CYP) inhibition (CYP2C9, CYP2C19, CYP3A4), human ether-à-go-go-related gene models I and II (hERG I and II) channel inhibition, AMES mutagenicity, and hepatotoxicity. All six compounds were profiled under identical conditions.

3. Results

3.1. Docking scores and GC-376 benchmark

Predicted binding free energies are listed in Table 1 and visualized in Figure 2. Posaconazole ranked first at −8.288 kcal/mol, and itraconazole ranked second at −8.095 kcal/mol. The 0.19 kcal/mol gap between them is within AutoDock Vina's reported scoring uncertainty of ±0.5 kcal/mol[18] and does not constitute a meaningful distinction.

Table 1. Predicted binding free energies (ΔG) for all compounds docked against SARS-CoV-2 Mpro (PDB: 6LU7) using AutoDock Vina v1.2.5

Compound	MW (g/mol)	Molecular formula	ΔG (kcal/mol)	Rank	Notes
Posaconazole	700.79	$C_{37}H_{42}F_2N_8O_4$	−8.288	1	Test compound
Itraconazole	705.65	$C_{35}H_{38}Cl_2N_8O_4$	−8.095	2	Test compound
GC-376 (control)	523.58	$C_{22}H_{22}F_2N_4O_7S$	−6.763	3	Non-covalent benchmark
Fluconazole	306.28	$C_{13}H_{12}F_2N_6O$	−5.068	4	Test compound
Nirmatrelvir[a]	499.53	$C_{23}H_{32}F_3N_5O_4$	−4.370	5	Covalent reference
Ketoconazole	531.44	$C_{26}H_{28}Cl_2N_4O_4$	−3.769	6	Test compound

Notes: [a] Nirmatrelvir's rank reflects the absence of covalent bonding terms in Vina's scoring function, not an inherently weak affinity. Compounds ranked from most to least negative ΔG.
Abbreviation: MW: Molecular weight.

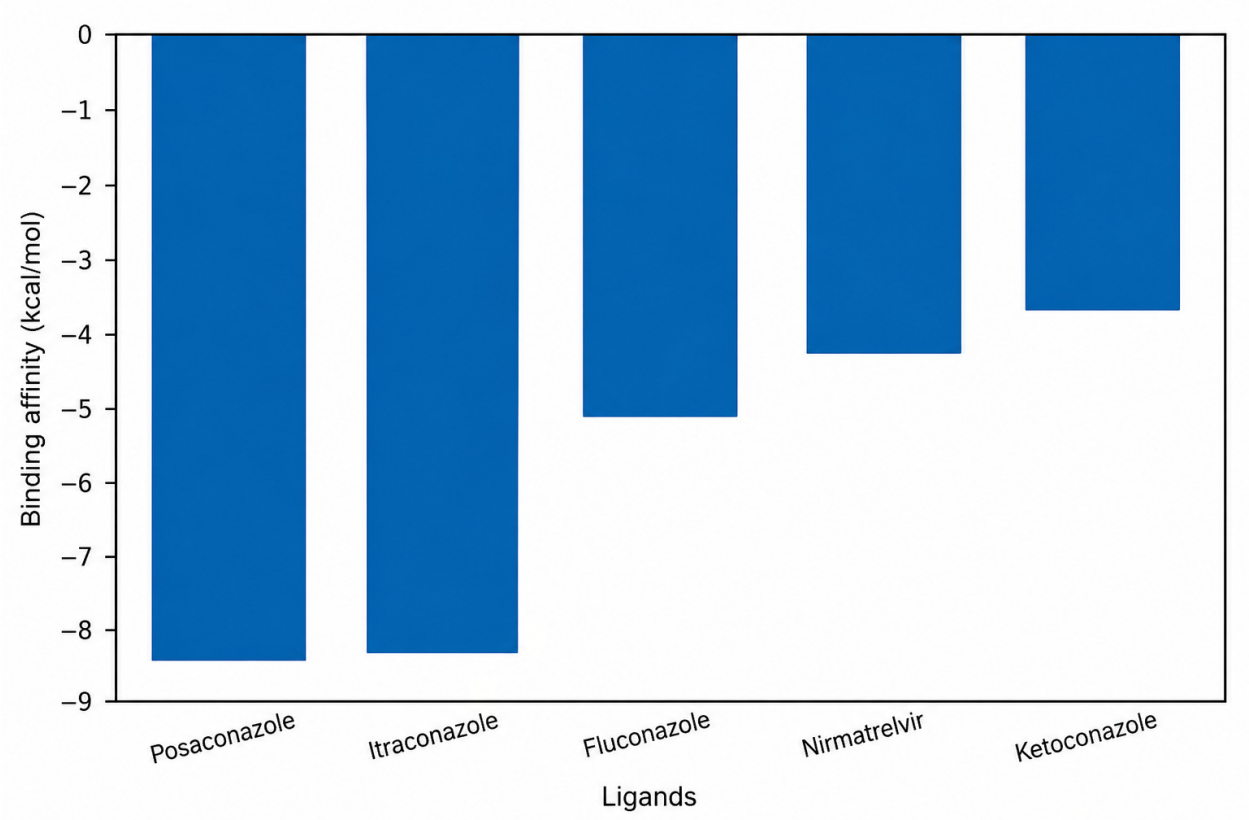


Figure 2. Predicted binding affinities (ΔG, kcal/mol) for all six compounds against SARS-CoV-2 main protease (Mpro). GC-376 (−6.763 kcal/mol) is the validated non-covalent reference. Nirmatrelvir's lower rank reflects the absence of covalent bonding terms in Vina's scoring function.

GC-376 scored −6.763 kcal/mol under the same rigid-receptor protocol.[11] This is the directly comparable non-covalent baseline with documented enzymatic IC_{50} data. Posaconazole and itraconazole exceeded it by ~1.5 kcal/mol. Whether that margin reflects better binding geometry, van der Waals surface-area inflation from their large MW, or both cannot be resolved from docking alone.

Fluconazole (−5.068 kcal/mol), nirmatrelvir (−4.370 kcal/mol), and ketoconazole (−3.769 kcal/mol) occupied the lower end. The MW–score dependence was straightforward: the two heaviest compounds (>700 g/mol) scored most negatively; the lightest (306 g/mol) did not. Nirmatrelvir's non-covalent rank does not indicate its clinical potency, which depends entirely on CYS145 alkylation.

3.2. Binding pose, active-site contacts, and estimated interaction distances

The top-ranked pose of posaconazole occupied the substrate-binding cleft, in contact with the HIS41-CYS145 catalytic dyad. The scaffold spanned ~27 Å along its longest axis, reaching the S1, S2, and S3 sub-pockets simultaneously (Figures 3 and 4). The terminal difluorophenyl group was oriented toward S2, with MET49 at an estimated C–S···π distance of ~3.8 Å. The central piperazinyl-triazolone segment approached GLU166 at an estimated polar contact distance of ~3.3 Å. Full residue assignments and estimated distances are in Table 2.

Estimated distances at the catalytic dyad were ~3.2 Å for HIS41, and ~3.5 Å for CYS145, both within typical polar contact and van der Waals ranges. MET165 (S3 sub-pocket) registered ~4.1 Å, consistent with a looser hydrophobic contact at the S3 periphery. LEU141, THR24, and THR26 fell between 4.3 and 4.8 Å; therefore, they were at the outer shell of the interaction radius.

All estimated distances in Table 2 were measured from the top-ranked rigid-docked pose using the PyMOL distance tool. They carry inherent coordinate uncertainty from the rigid-receptor approximation and are not experimentally validated geometries. They are reported to provide approximate spatial context for the interaction assignments, not as precise molecular measurements. Crystallographic characterization or molecular dynamics

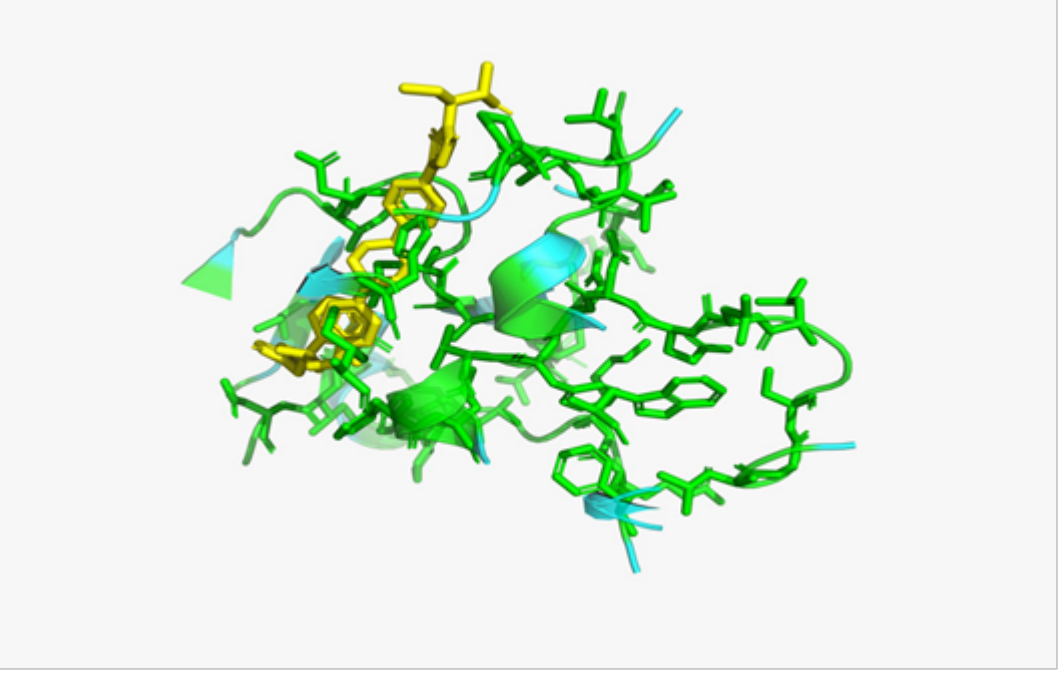


Figure 3. PyMOL rendering of the posaconazole–main protease (Mpro)-docked complex. Posaconazole (yellow sticks) is positioned within the HIS41-CYS145 catalytic cleft. Active-site residues within ~5 Å are shown in green sticks.

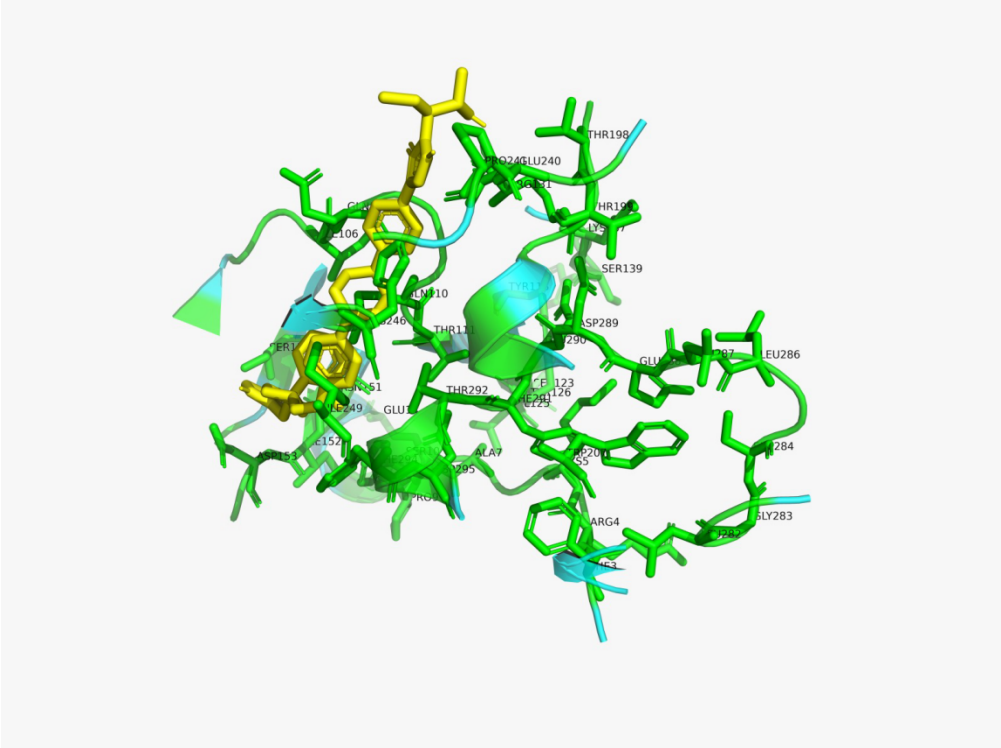


Figure 4. Labeled residue-interaction view of the posaconazole-main protease (Mpro) complex. Key residues (HIS41, CYS145, MET49, MET165, GLU166, LEU141, THR24, THR26) are annotated. Rendered in PyMOL v2.5 from the same AutoDock Vina top-ranked pose as Figure 3.

(MD)-equilibrated coordinates would be required to validate them.

3.3. Drug-likeness and Lipinski compliance

SwissADME data are shown in Table 3. Fluconazole and nirmatrelvir satisfied all Lipinski criteria. Ketoconazole incurred a single violation from MW marginally above 500 g/mol. Posaconazole and itraconazole violated three criteria each: MW exceeding 700 g/mol, logP above 4.5, and HBA at or near the limit of 10. Both fit a Biopharmaceutics Classification System (BCS) Class II profile; their approved clinical formulations compensate for this by using cyclodextrin complexation or lipid-based vehicles. GC-376 violated only the MW threshold at 523.58 g/mol.

3.4. Absorption, distribution, metabolism, excretion, and toxicity profiling

The results of pkCSM are shown in Table 4. A comparative summary of ADMET and drug-likeness properties for all evaluated compounds is presented in Table 5. Fluconazole produced the cleanest profile: no hERG I or II inhibition, no hepatotoxicity flag, no AMES mutagenicity, and negative P-gp substrate status, consistent with its clinical safety record.

Nirmatrelvir carried a hepatotoxicity flag from pkCSM. Given the compound's acceptable hepatic profile in Paxlovid® trials, this is likely a classifier error.[23] The false-positive rate for pkCSM's hepatotoxicity classifier on structurally diverse test sets illustrates why single-platform ADMET predictions should not be treated as definitive.

Posaconazole and itraconazole generated hERG II inhibition predictions and hepatotoxicity flags. Both carry Q–T prolongation warnings in their clinical prescribing information, so the hERG predictions align with known pharmacology. Ketoconazole's CYP3A4 and hepatotoxicity entries are not predictions—they are established liabilities that led to its systemic withdrawal in multiple jurisdictions.[24] GC-376 showed a clean ADMET profile.[11]

4. Discussion

4.1. Interpretation of the GC-376 benchmark and scoring inflation

The 1.5 kcal/mol margin of posaconazole and itraconazole over GC-376 should be interpreted with caution before drawing any firm conclusions. GC-376 is a bisulfite prodrug that inhibits Mpro non-covalently with an IC_{50} in the low micromolar range[11]—a value reproduced in enzymatic and cellular assays. Its −6.763 kcal/mol score under this protocol is a grounded reference point. Any compound exceeding it substantially is either binding with genuinely superior geometry, forming van der Waals contacts through molecular bulk, or both.

The MW–score correlation across this dataset is significant. AutoDock Vina assigns van der Waals energy as a function of contact surface area; larger molecules accumulate more contacts by simple geometry.[18] A solvation correction or logP-adjusted regression would partially deflate this inflation.[12] Without one, the 1.5 kcal/mol gap cannot be interpreted as superior enzymatic potency. It might even close or reverse once desolvation costs associated with posaconazole's lipophilic surface are properly accounted for.

4.2. Rigid-receptor limitations for SARS-CoV-2 main protease

The S2 loop (residues 45–52) shows meaningful positional variation across deposited Mpro crystal structures.[4] Freezing it in a rigid-receptor calculation either overstates or understates binding accessibility, depending on the direction of loop movement upon ligand binding. GLU166 has lower positional variance, and its predicted contact is less likely to be a rigid-receptor artifact.[4] THR24 and THR26 vary more; those peripheral contacts should be treated with corresponding caution.[25]

Entropy is a second gap. Posaconazole has seven rotatable bonds between its ring systems. Vina penalizes these torsions, but that penalty potentially underestimates the actual entropy cost of immobilizing a scaffold of this conformational complexity. Molecular mechanics/Poisson–Boltzmann surface area (MM/PBSA) or molecular mechanics/generalized born surface area (MM/GBSA) rescoring on MD trajectories would provide a more rigorous treatment.[26] Ensemble docking across multiple deposited Mpro conformers[27] would address receptor flexibility with substantially less computational overhead than full induced-fit docking.

4.3. Structural basis of posaconazole's predicted affinity

Posaconazole's four-ring systems span ~27 Å—enough to engage S1, S2, and S3 simultaneously. The estimated distances at MET49 (~3.8 Å, C–S···π), MET165 (~4.1 Å), and GLU166 (~3.3 Å) are within the ranges reported for corresponding contacts in Mpro co-crystal structures,[4] which gives the pose face validity. HIS41 (~3.2 Å) and CYS145 (~3.5 Å) fall within typical polar contact distances at the catalytic dyad.

Face validity is not structural proof. All estimated distances in Table 2 were derived from a rigid-receptor model and were accompanied by ±0.3–0.5 Å coordinate uncertainty. Whether these contacts persist on the

Table 2. Active-site residues within the posaconazole–Mpro binding cleft

Residue	Functional region	Interaction type	Estimated distance (Å)[a]	Functional significance
HIS41	Catalytic dyad	Polar/π-stacking	~3.2	Catalytic site engagement; imidazole nitrogen within polar contact range of triazolone oxygen
CYS145	Catalytic dyad	Polar/van der Waals	~3.5	Catalytic site engagement; sulfhydryl within van der Waals contact of difluorophenyl edge
MET49	S2 sub-pocket	Hydrophobic (C–S···π)	~3.8	Hydrophobic packing; sulfur within C–S···π range of triazole ring; well-documented in co-crystal structures[4]
MET165	S3 sub-pocket	Hydrophobic (C–S···π)	~4.1	Hydrophobic packing; S3 contributor; longer contact distance consistent with peripheral engagement
GLU166	Substrate recognition	Polar/electrostatic	~3.3	P1-glutamine mimicry contact; backbone carbonyl within polar interaction range; geometry unconfirmed without crystallography or MD
LEU141	S1 sub-pocket	Hydrophobic/van der Waals	~4.3	Backbone anchoring at the S1 boundary
THR24	S4 sub-pocket	Polar/van der Waals	~4.8	Peripheral contact; modest enthalpic contribution expected
THR26	S4 sub-pocket	Polar/van der Waals	~4.6	Peripheral contact; modest enthalpic contribution expected

Notes: [a]All distances are rigid-docking estimates (±0.3–0.5 Å approximate uncertainty). Crystallographic or MD validation is required before these values can be interpreted as true binding geometries. Estimated distances (Å) were measured from the rigid-docked pose in PyMOL v2.5 and carry inherent coordinate uncertainty; they are approximate spatial references, not experimentally validated bond geometries.[4]
Abbreviations: MD: Molecular dynamics; Mpro: Main protease.

Table 3. Drug-likeness and Lipinski rule-of-five (RO5) parameters from SwissADME

Compound	MW	LogP	HBD	HBA	TPSA (Å²)	RO5 violation	GI absorption	Oral bioavailability
Posaconazole	700.79	4.57	1	10	120.7	3 (multiple)	High	Poor
Itraconazole	705.65	5.58	0	10	98.2	3 (multiple)	High	Poor
GC-376	523.58	1.80	3	9	142.6	1 (MW)	Moderate	Moderate
Fluconazole	306.28	0.73	1	7	81.6	0	High	Good
Nirmatrelvir	499.53	1.10	3	7	138.6	0	High	Moderate
Ketoconazole	531.44	3.71	0	7	87.0	1 (MW)	High	Moderate

Notes: GI absorption from brain or intestinal estimated permeation method (BOILED)-Egg model predictions. RO5 Viol. = Lipinski violations
Abbreviations: GI: Gastrointestinal; HBA: Hydrogen bond acceptors; HBD: Hydrogen bond donors; MW: Molecular weight; TPSA: Topological polar surface area.

Table 4. ADMET properties predicted by pkCSM

Compound	GI absorption	P-gp substrate	CYP3A4 inhibition	hERG I	hERG II	AMES	Hepatotoxicity	Notes
Posaconazole	High	Y[a]	Y[a]	N	Y[a]	N	Y[a]	-
Itraconazole	High	Y[a]	Y[a]	N	Y[a]	N	Y[a]	-
GC-376	Moderate	N	N	N	N	N	N	-
Fluconazole	High	N	N	N	N	N	N	Cleanest profile
Nirmatrelvir	High	N	N	N	N	N	Y[b]	-
Ketoconazole	High	Y[a]	Y[a]	N	Y[a]	N	Y[a]	Clinically confirmed[25]

Notes: [a]Predicted safety liabilities. [b]Probably false positive.[23] Y = Predicted positive; N = Predicted negative.
Abbreviations: ADMET: Absorption, distribution, metabolism, excretion, and toxicity; GI: Gastrointestinal; hERG: Human ether-à-go-go-related gene; P-gp: P-glycoprotein.

Table 5. Comparative ADMET and drug-likeness summary of the selected ligands

Ligand	MW	LogP	GI absorption	Lipinski violations	hERG risk	Hepatotoxicity
Posaconazole	700.79	4.57	High	3	Yes	Yes
Itraconazole	705.65	5.58	High	3	Yes	Yes
Fluconazole	306.28	0.73	High	0	No	No
Ketoconazole	531.44	3.71	High	1	Yes	Yes
Nirmatrelvir	499.53	1.10	High	0	No	Yes

Abbreviations: ADMET: Absorption, distribution, metabolism, excretion, and toxicity; GI: Gastrointestinal; hERG: Human ether-à-go-go-related gene; MW: Molecular weight.

nanosecond timescale of enzyme–inhibitor encounter requires MD trajectories. Root-mean-square deviation (RMSD) monitoring of ligand heavy atoms and per-residue contact frequency analysis across a 100–200 ns simulation would quantify pose stability in a way that the static Vina result cannot.

4.4. Fluconazole: The absorption, distribution, metabolism, excretion, and toxicity (ADMET)-tractable scaffold

Fluconazole scored 1.7 kcal/mol less than GC-376. Its MW of 306 g/mol and logP of 0.73 limit hydrophobic surface contact with S2 and S3, representing a real affinity liability. It also reported no RO5 violations, no hERG II inhibition,

no CYP3A4 inhibition, no hepatotoxicity flag, and decades of clinical safety data.

Even a modest experimental IC_{50} against Mpro would make fluconazole substantially more tractable than either of the high-scoring azoles. Its small size creates a medicinal chemistry entry point: fragment growing toward S2, guided by the posaconazole pose as a pharmacophore model, could improve affinity without discarding the favorable physicochemical properties. This pathway is developed further in Section 4.9.

4.5. The affinity–pharmacokinetics trade-off

The inversion between docking rank and ADMET profile is not a quirk of this dataset. Potency optimization tends to increase lipophilicity, which drives docking scores higher while worsening solubility, elevating plasma protein binding, increasing metabolic liability, and increasing the risk of cardiac channel interactions.[12]

COVID-19 patients are frequently elderly and on multiple medications. Both posaconazole and itraconazole are robust CYP3A4 inhibitors, requiring careful management when used alongside antiretrovirals, antihypertensives, and anticoagulants that patients commonly receive.[9] They have also been reported with Q–T prolongation warnings. Ketoconazole's trajectory from a useful antifungal to a systemically withdrawn drug illustrates where those liabilities lead when not resolved.[24] A score of −8.3 kcal/mol with three Lipinski violations and hERG activity leads to a substantially more costly development path than a score of −5.1 kcal/mol with a clean safety profile.

4.6. Covalent docking and nirmatrelvir

Nirmatrelvir's fifth-place ranking reflects the design of the protocol, not the compound's potency. Covalent bond formation with CYS145 contributes −5 to −10 kcal/mol, which Vina cannot score.[18] The −4.370 kcal/mol value captures only the non-covalent complementarity of the non-warhead portion against the frozen receptor. Future studies that aim to use nirmatrelvir as a direct affinity comparator should use covalent docking tools—CovDock, FITTED, or AutoDock4 with covalent constraints—capable of scoring the thioimidate intermediate.

4.7. Absorption, distribution, metabolism, excretion, and toxicity prediction reliability and consensus validation

SwissADME and pkCSM are established platforms with well-documented performance in the drug-like chemical space, but their classifiers are machine-learning models trained on finite training sets and exhibit classifier-specific false-positive rates that can exceed 20% on structurally diverse compounds.[20,23] Nirmatrelvir's hepatotoxicity flag—from a compound with a clean hepatic profile in large COVID-19 trials—is a concrete example.

Single-platform ADMET predictions are risk-stratification signals, not pharmacokinetic verdicts. Future work on any scaffold prioritized from this study should incorporate multi-platform toxicity consensus modeling. Tools such as ProTox-II and SwissTox operate on partially independent training sets and feature representations; hepatotoxicity and hERG predictions that converge across two or three such platforms carry substantially higher confidence than single-platform outputs. This is a recommendation for follow-up validation, not a claim that consensus modeling was performed here. In vitro confirmation (metabolic stability assays, plasma protein binding measurements, hERG patch-clamp electrophysiology) remains the definitive validation step regardless of computational consensus.

4.8. Limitations

Six methodological limitations bound the interpretive scope of these findings:

(i) Rigid receptor model. Induced-fit effects at the S2 loop (residues 45–52) are not captured. The frozen receptor may overstate or understate binding accessibility for bulky ligands. Ensemble docking against multiple Mpro conformers would produce more reliable rank-ordering.

(ii) No MD simulation. Docked poses are static. Pose stability at physiological temperature and the time evolution of binding contacts cannot be assessed without MD trajectories.

(iii) No binding free energy calculations. Vina ΔG values carry ± 0.5–1.0 kcal/mol uncertainty.[18] MM/PBSA or MM/GBSA rescoring on MD trajectories would produce more rigorous estimates.

(iv) Interaction distances are rigid-docking estimates. Distances in Table 2 were measured from a rigid-receptor pose in PyMOL and carry ± 0.3–0.5 Å coordinate uncertainty. They are not experimentally validated geometries.

(v) Covalent mechanism not modeled. Nirmatrelvir's CYS145 alkylation mechanism cannot be scored by Vina. GC-376 is the primary non-covalent benchmark throughout.

(vi) No experimental data. No enzyme inhibition assay, cellular antiviral experiment, or in vivo data were generated. Every result is a computational hypothesis. No antiviral activity is claimed.

4.9. Future perspectives

The most immediate computational step is MD simulation (100–200 ns, GROMACS v2022 or AMBER22, CHARMM36m force field, explicit TIP3P solvent, Particle Mesh Ewald electrostatics) of the posaconazole–Mpro and fluconazole–Mpro docked complexes. RMSD monitoring of ligand heavy atoms and per-residue contact frequency analysis would clarify which Vina-predicted contacts persist dynamically. If any contacts are stable, the same trajectories would support MM/PBSA rescoring with solvation contributions accounted for.[26] Ensemble docking against multiple deposited Mpro conformers would address receptor flexibility more tractably than full induced-fit docking.

The most useful next experimental step is a Förster resonance energy transfer (FRET)-based Mpro inhibition assay with recombinant enzyme and a fluorogenic substrate. A dose-response IC_{50} for fluconazole—however modest—would either validate or refute the docking result. Selectivity profiling against cathepsins B and L would establish discrimination against related human cysteine proteases. Cell-based antiviral evaluation (cytopathic effect or plaque-reduction assay) would follow a confirmed enzymatic result using Vero E6 or Calu-3 cells.

In optimizing fluconazole, the posaconazole binding pose identifies two attachment vectors worth exploring. The S2 sub-pocket contacts at MET49 (~3.8 Å) and MET165 (~4.1 Å) represent the largest affinity gap between fluconazole and the higher-scoring azoles. Appending a cyclopentyl group to the para-position of one of fluconazole's fluorophenyl rings would add a compact hydrophobic substituent (~71 Da) directly into this pocket. An isopropyl group would achieve similar pocket occupancy with a smaller MW increment (~42 Da). Both modifications would increase logP from the current 0.73—potentially by 0.8–1.2 units, depending on the substitution position—but would keep logP well within the Lipinski limit of 5, provided no other changes are made to the scaffold. TPSA, currently 81.6 $Å^2$, would increase only marginally with either substitution and remain far below the 140 $Å^2$ threshold associated with poor oral absorption.

The GLU166 contact (~3.3 Å estimated) is a secondary pharmacophore anchor. A short hydrogen-bond donor—a hydroxymethyl or aminomethyl group attached to the triazole ring—could reinforce this contact while adding modest MW. The combined scaffold (fluconazole + hydrophobic S2 fragment + GLU166-directed polar group) would be estimated to weigh 420–450 g/mol, well within RO5, and could be synthesized from fluconazole as a starting material through directed ortho-metalation or palladium-catalyzed cross-coupling. Computationally, the modified scaffold should be docked and rescored under the same Vina protocol before any synthesis is committed to, with particular attention to whether the added hydrophobic fragment maintains the GLU166 polar contact in the top-ranked pose.

For posaconazole and itraconazole, optimization would require reducing logP from >4.5 to <3.0 through ring saturation or polar group introduction, attenuating hERG II activity, and preserving the multi-point binding geometry. An analogue search across commercially available antifungal derivatives in PubChem or ChEMBL, filtered for logP < 3.5 and MW < 550 g/mol, docked under the same protocol, could identify better-balanced starting points before synthetic investment.

Future ADMET evaluation of any optimized scaffold should use multi-platform consensus modeling (ProTox-II, SwissTox, and pkCSM in parallel) to reduce the risk of single-classifier false positives before in vitro toxicity screening is initiated.

5. Conclusion

Four antifungal azoles were evaluated against SARS-CoV-2 Mpro, alongside GC-376 (−6.763 kcal/mol, non-covalent benchmark) and nirmatrelvir (covalent mechanistic reference), using AutoDock Vina v1.2.5 under a uniform rigid-receptor protocol. Posaconazole (−8.288 kcal/mol) and itraconazole (−8.095 kcal/mol) reported the highest predicted affinities, with poses spanning the HIS41-CYS145 catalytic cleft and estimated interaction distances at MET49 (~3.8 Å), MET165 (~4.1 Å), and GLU166 (~3.3 Å). These distances are rigid-docking estimates, not experimentally validated geometries. The ~1.5 kcal/mol margin over GC-376 includes scoring inflation from MW and cannot be equated with greater enzymatic potency without experimental IC_{50} data.

Both high-scoring compounds carry multiple Lipinski violations, hERG II inhibition risk, CYP3A4 inhibitory liability, and hepatotoxicity flags already evident in their approved clinical use. Fluconazole, weaker on the docking metric, has a fully RO5-compliant ADMET profile, no cardiac channel risk, and decades of clinical safety data—making it the most tractable starting point for experimental follow-up and scaffold optimization. Ketoconazole ranked last on both docking affinity and pharmacokinetic safety, and is the weakest repurposing candidate in this series.

No antiviral activity is claimed. All findings are computational hypotheses requiring confirmation through MD simulation, binding free energy estimation, an Mpro enzymatic IC_{50} assay, and cell-based antiviral testing. Future work should also incorporate multi-platform

ADMET consensus modeling to reduce single-classifier prediction uncertainty. The protocol and dataset here provide a reproducible, conservatively interpreted baseline for those next experiments.

Acknowledgments

The author acknowledges the use of publicly available computational tools and databases, including PubChem, AutoDock Vina, SwissADME, pkCSM, Open Babel, MGLTools, and PyMOL for conducting this study. The author also acknowledges Mahrukh Zainab, a BS English student, for assistance in language refinement and manuscript readability improvement.

Funding

None.

Conflict of interest

The author declares no competing financial or non-financial interests in relation to the work described in this manuscript.

Author contributions

This is a single-authored article.

Ethical approval and consent to participate

Not applicable.

Consent for publication

Not applicable.

Availability of data

The datasets generated and analyzed during the current study, including prepared ligand and protein PDBQT files, AutoDock Vina configuration files, docking output logs, and SwissADME/pkCSM prediction reports, are available from the corresponding author upon reasonable request.

References

1. Zhou P, Yang XL, Wang XG, *et al.* A pneumonia outbreak associated with a new coronavirus of probable bat origin. *Nature*. 2020;579(7798):270-273.

   doi: 10.1038/s41586-020-2012-7

2. Ziebuhr J, Snijder EJ, Gorbalenya AE. Virus-encoded proteinases and proteolytic processing in the Nidovirales. *J Gen Virol*. 2000;81(Pt 4):853-879.

   doi: 10.1099/0022-1317-81-4-853

3. Hegyi A, Ziebuhr J. Conservation of substrate specificities among coronavirus main proteases. *J Gen Virol*. 2002;83(Pt 3):595-599.

   doi: 10.1099/0022-1317-83-3-595

4. Zhang L, Lin D, Sun X, *et al.* Crystal structure of SARS-CoV-2 main protease provides a basis for design of improved alpha-ketoamide inhibitors. *Science*. 2020;368(6489):409-412.

   doi: 10.1126/science.abb3405

5. Jin Z, Du X, Xu Y, *et al.* Structure of Mpro from SARS-CoV-2 and discovery of its inhibitors. *Nature*. 2020;582(7811):289-293.

   doi: 10.1038/s41586-020-2223-y

6. Owen DR, Allerton CMN, Anderson AS, *et al.* An oral SARS-CoV-2 Mpro inhibitor clinical candidate for the treatment of COVID-19. *Science*. 2021;374(6575):1586-1593.

   doi: 10.1126/science.abl4784

7. Pushpakom S, Iorio F, Eyers PA, *et al.* Drug repurposing: progress, challenges and recommendations. *Nat Rev Drug Discov*. 2019;18(1):41-59.

   doi: 10.1038/nrd.2018.168

8. Hof H. A new, broad-spectrum azole antifungal: posaconazole—mechanisms of action and resistance, spectrum of activity. *Mycoses*. 2006;49(Suppl 1):2-6.

   doi: 10.1111/j.1439-0507.2006.01295.x

9. Bruggemann RJM, Alffenaar JWC, Blijlevens NMA, *et al.* Clinical relevance of pharmacokinetic interactions of azole antifungal drugs with other coadministered agents. *Clin Infect Dis*. 2009;48(10):1441-1458.

   doi: 10.1086/598327

10. Ghosh R, Chakraborty A, Biswas A, Chowdhuri S. Identification of polyphenols from Broussonetia papyrifera as SARS-CoV-2 main protease inhibitors using in silico docking and molecular dynamics simulation approaches. *J Biomol Struct Dyn*. 2021;39(17):6747-6760.

    doi: 10.1080/07391102.2020.1802347

11. Ma C, Sacco MD, Hurst B, *et al.* Boceprevir, GC-376, and calpain inhibitors II, XII inhibit SARS-CoV-2 viral replication by targeting the viral main protease. *Cell Res*. 2020;30(8):678-692.

    doi: 10.1038/s41422-020-0356-z

12. Leeson PD, Springthorpe B. The influence of drug-like concepts on decision-making in medicinal chemistry. *Nat Rev Drug Discov*. 2007;6(11):881-890.

    doi: 10.1038/nrd2445

13. Berman HM, Westbrook J, Feng Z, *et al.* The Protein Data Bank. *Nucleic Acids Res*. 2000;28(1):235-242.

    doi: 10.1093/nar/28.1.235

14. Liu X, Zhang B, Jin Z, Yang H, Rao Z. The crystal structure of COVID-19 main protease in complex with an inhibitor

N3. *RCSB PDB*. 2020.

doi: 10.2210/pdb6LU7/pdb

15. Morris GM, Huey R, Lindstrom W, *et al.* AutoDock4 and AutoDockTools4: automated docking with selective receptor flexibility. *J Comput Chem*. 2009;30(16):2785-2791.

doi: 10.1002/jcc.21256

16. Kim S, Chen J, Cheng T, *et al.* PubChem in 2021: new data content and improved web interfaces. *Nucleic Acids Res*. 2021;49(D1):D1388-D1395.

doi: 10.1093/nar/gkaa971

17. O'Boyle NM, Banck M, James CA, Morley C, Vandermeersch T, Hutchison GR. Open Babel: an open chemical toolbox. *J Cheminform*. 2011;3:33.

doi: 10.1186/1758-2946-3-33

18. Eberhardt J, Santos-Martins D, Tillack AF, Forli S. AutoDock Vina 1.2.0: new docking methods, expanded force field, and Python bindings. *J Chem Inf Model*. 2021;61(8):3891-3898.

doi: 10.1021/acs.jcim.1c00203

19. Schrödinger LLC. *The PyMOL Molecular Graphics System, Version 2.5*. New York, NY; 2021. https://www.pymol.org

20. Daina A, Michielin O, Zoete V. SwissADME: a free web tool to evaluate pharmacokinetics, drug-likeness and medicinal chemistry friendliness of small molecules. *Sci Rep*. 2017;7:42717.

doi: 10.1038/srep42717

21. Lipinski CA, Lombardo F, Dominy BW, Feeney PJ. Experimental and computational approaches to estimate solubility and permeability in drug discovery and development settings. *Adv Drug Deliv Rev*. 2001;46(1-3):3-26.

doi: 10.1016/S0169-409X(00)00129-0

22. Daina A, Zoete V. A BOILED-Egg to predict gastrointestinal absorption and brain penetration of small molecules. *Chem Med Chem*. 2016;11(11):1117-1121.

doi: 10.1002/cmdc.201600182

23. Pires DEV, Blundell TL, Ascher DB. pkCSM: predicting small-molecule pharmacokinetic and toxicity properties using graph-based signatures. *J Med Chem*. 2015;58(9):4066-4072.

doi: 10.1021/acs.jmedchem.5b00104

24. European Medicines Agency. Ketoconazole-containing medicines: referral. 2013. Accessed May 2026. https://www.ema.europa.eu/en/medicines/human/referrals/ketoconazole-containing-medicines

25. Sanguinetti MC, Tristani-Firouzi M. hERG potassium channels and cardiac arrhythmia. *Nature*. 2006;440(7083):463-469.

doi: 10.1038/nature04710

26. Genheden S, Ryde U. The MM/PBSA and MM/GBSA methods to estimate ligand-binding affinities. *Expert Opin Drug Discov*. 2015;10(5):449-461.

doi: 10.1517/17460441.2015.1032936

27. Ferreira LG, Dos Santos RN, Oliva G, Andricopulo AD. Molecular docking and structure-based drug design strategies. *Molecules*. 2015;20(7):13384-13421.

doi: 10.3390/molecules200713384